Publication I

K. Uusi-Esko, J. Malm, N. Imamura, H. Yamauchi, M. Karppinen, Characterization of *R*MnO_3 (*R* = Sc, Y, Dy-Lu): High-Pressure Synthesized Metastable Perovskites and Their Hexagonal Precursor Phases, Mater. Chem. Phys. 112 (2008) 1029-1034.

Materials Chemistry and Physics 112 (2008) 1029–1034

Contents lists available at ScienceDirect

Materials Chemistry and Physics

journal homepage: www.elsevier.com/locate/matchemphys

Characterization of RMnO$_3$ (R = Sc, Y, Dy-Lu): High-pressure synthesized metastable perovskites and their hexagonal precursor phases

K. Uusi-Esko[a,b], J. Malm[b], N. Imamura[a], H. Yamauchi[a], M. Karppinen[a,b,*]

[a] Materials and Structures Laboratory, Tokyo Institute of Technology, Yokohama 226-8503, Japan
[b] Laboratory of Inorganic Chemistry, Department of Chemistry, Helsinki University of Technology, P.O. Box 6100, FI-02015 TKK, Finland

ARTICLE INFO

Article history:
Received 21 February 2008
Received in revised form 9 May 2008
Accepted 1 July 2008

Keywords:
High-pressure synthesis
Manganate oxides

ABSTRACT

A series of RMnO$_3$ samples with R = Sc, Y, Dy-Lu was synthesized through a two-step route in which first the hexagonal oxides, h-RMnO$_3$, were prepared under normal pressure using an EDTA method and then converted to orthorhombic perovskites, o-RMnO$_3$, through a high-pressure treatment at 5 GPa and 800 °C. Since all the aforementioned members but the R = Sc member were converted to an orthorhombic perovskite phase under the 5-GPa high-pressure condition, an additional sample of InMnO$_3$ of the hexagonal structure was prepared and tested for the high-pressure conversion. The stability limit of the orthorhombic perovskite structure under the 5-GPa high-pressure condition was concluded to be located between InMnO$_3$ and LuMnO$_3$ in terms of the size of the A-site cation constituent, R^{III} or In^{III}. The decrease in the size of R^{III} was found to increase the distortion of o-RMnO$_3$ with a decrease in the Mn—O—Mn bond angle from 144.3° for Dy to 140.3° for Lu. All the hexagonal and orthorhombic RMnO$_3$ phases exhibited antiferromagnetic characteristics at low temperatures.

1. Introduction

Manganese oxides of the general formula RMnO$_3$ (R = rare-earth element) have been intensely studied in recent years owing to the exciting properties they possess, such as the colossal magnetoresistance (CMR) and multiferroic effects [1–6]. The potential applications of CMR materials include magnetic sensors and read heads [7]. Multiferroic magnetoelectrics, on the other hand, are especially appealing because in addition to their ferromagnetic and ferroelectric properties, they often possess additional functionalities due to couplings between the magnetic and electric polarizations. Along with the current trend of device miniaturization, these kinds of multifunctional materials have become increasingly attractive, as they may enable the fabrication of device components that can perform more than just one task [8].

The RMnO$_3$ system is structurally divided into two subsystems. For the larger rare earths, R = La-Dy, an orthorhombically distorted perovskite structure (*Pbnm*) is adopted, *i.e.* o-RMnO$_3$, whereas for the smaller rare earths, R = Sc, Y and Ho-Lu, the structure is hexagonal ($P6_3cm$), *i.e.* h-RMnO$_3$ [9,10]. However, it is possible to prepare metastable orthorhombic perovskites of the smaller Rs under high pressures [11,12] or by means of other special synthesis methods, such as low-temperature soft chemistry [13–15] or epitaxial thin-film growth [16,17]. The hexagonal structure of the smaller Rs can be described as layers of Mn-centered trigonal bipyramids of MnO$_5$ that are separated by a layer of trivalent R cations [18]. The MnO$_5$ bipyramids are tilted and shifted relative to the R^{III} ions, *i.e.* the structure is noncentrosymmetric. This is the reason for the ferroelectric polarization observed along the c axis in h-RMnO$_3$. The h-RMnO$_3$ compounds are also magnetic with an antiferromagnetic (AFM) ordering of the Mn^{III} moments [19]. The ferroelectric transition occurs at high temperatures and the antiferromagnetic transition of the Mn^{III} moments at low temperatures. These two types of ordering coexist at low temperatures and thus the h-RMnO$_3$ compounds are multiferroic. In the orthorhombically deformed perovskite structure of the larger Rs, the trivalent Mn cations are located inside corner-sharing MnO$_6$ octahedra [15,19,20]. The members of the o-RMnO$_3$ perovskite subsystem are AFM insulators below their Néel temperatures (T_N), but the spin configuration changes with the rare-earth species [21]. Hole-doping is needed to make the CMR phenomenon occur in the o-RMnO$_3$ perovskites [22,23].

There is a rather large difference in the size of the two smallest rare earths, *i.e.* lutetium and scandium. Interestingly, hexagonal InMnO$_3$ is isostructural with h-RMnO$_3$ [24,25] and the ionic radius of trivalent indium is between those of Sc^{III} and Lu^{III}. The synthesis of h-InMnO$_3$ was reported already in 1992 by Giaquinta and Zur-Loye [24], but the perovskite phase of InMnO$_3$ has not been

* Corresponding author. Tel.: +358 9 451 2600; fax: +358 9 462 373.
E-mail address: maarit.karppinen@tkk.fi (M. Karppinen).

0254-0584/$ – see front matter © 2008 Elsevier B.V. All rights reserved.
doi:10.1016/j.matchemphys.2008.07.009

Table 1
Lattice parameters and atomic positions of the hexagonal ($P6_3cm$) and perovskite ($Pbnm$) phases of RMnO$_3$ and InMnO$_3$ series from XRD data

		Dy	Ho	Y	Er	Tm	Yb	Lu	In	Sc
Hexagonal ($P6_3cm$)										
a (Å)			6.1518(0)	6.1483(0)	6.1215(0)	6.0927(0)	6.0682(0)	6.0467(0)	5.8770(0)	5.8308(0)
c (Å)			11.4131(0)	11.3993(0)	11.4101(0)	11.3908(0)	11.3695(0)	11.3719(0)	11.4767(0)	11.1763(0)
V (Å^3)			374.06(3)	373.18(2)	370.29(2)	366.18(2)	362.57(2)	360.08(2)	343.29(3)	329.07(3)
R1	2a(0,0,z)									
z			0.283(1)	0.271(1)	0.276(1)	0.278(2)	0.279(1)	0.284(1)		
R2	4b(1/3, 2/3, z)									
z			0.242(1)	0.231(1)	0.234(1)	0.236(2)	0.237(1)	0.241(1)		
Mn	6c (x,0,0)									
x			0.333(2)	0.349(1)	0.344(1)	0.343(1)	0.344(1)	0.339(1)		
O1	6c (x,0,z)									
x			0.300(2)	0.293(2)	0.289(2)	0.298(2)	0.305(4)	0.300(2)		
z			0.145(1)	0.152(1)	0.152(2)	0.151(1)	0.178(1)	0.157(2)		
O2	6c (x,0,z)									
x			0.643(3)	0.657(2)	0.645(2)	0.642(2)	0.642(3)	0.634(2)		
z			0.323(1)	0.327(1)	0.327(1)	0.324(1)	0.347(1)	0.327(2)		
O3	2a (0,0,z)									
z			0.498(2)	0.482(2)	0.491(2)	0.488(2)	0.485(4)	0.491(3)		
O4	4b(1/3, 2/3, z)									
z			0.037(2)	0.023(1)	0.025(1)	0.025(2)	0.023(3)	0.029(2)		
R_{wp} (%)			10.1	12.0	7.9	6.4	9.8	8.5		
Perovskite ($Pbnm$)										
a (Å)		5.2794(2)	5.2565(3)	5.2580(2)	5.2405(2)	5.2310(1)	5.2190(1)	5.1993(2)		
b (Å)		5.8430(2)	5.8329(3)	5.8361(2)	5.8228(3)	5.8157(1)	5.8038(1)	5.7906(2)		
c (Å)		7.3794(3)	7.3602(4)	7.3571(3)	7.3436(3)	7.3218(1)	7.3027(2)	7.2987(3)		
V (Å^3)		227.63(1)	225.67(2)	225.76(2)	224.09(2)	222.74(1)	221.20(1)	219.74(1)		
R	4c(x,y, 1/4)									
x		0.982(0)	0.981(0)	0.981(0)	0.9812(2)	0.982(0)	0.982(0)	0.981(0)		
y		0.082(0)	0.083(0)	0.084(0)	0.084(0)	0.085(0)	0.085(0)	0.086(0)		
Mn	4b (1/2,0,0)									
O1	4c (x,y, 1/4)									
x		0.108(2)	0.102(2)	0.115(1)	0.111(1)	0.111(2)	0.114(2)	0.121(2)		
y		0.471(2)	0.471(2)	0.465(1)	0.468(1)	0.468(2)	0.468(2)	0.469(2)		
O2	8d (x,y,z)									
x		0.707(1)	0.711(1)	0.700(1)	0.705(1)	0.704(1)	0.707(2)	0.713(2)		
y		0.328(1)	0.328(1)	0.326(1)	0.327(1)	0.326(1)	0.328(2)	0.330(2)		
z		0.052(1)	0.052(1)	0.053(1)	0.053(1)	0.056(1)	0.057(1)	0.062(1)		
R_{wp} (%)		13.6	10.2	8.3	8.4	10.2	15.2	16.4		
Mn–O1–Mn		144.3	145.7	141.7	143.2	143.2	142.0	140.3		
Mn–O2–Mn		145.6	146.1	144.5	144.9	144.2	144.1	143.5		
'Mn–O–Mn'		144.9	145.9	143.1	144.1	143.7	143.0	141.9		

The standard deviations are given in parentheses.

synthesized and therefore it is exciting to see if it could be prepared in the same manner as the RMnO$_3$ series, *i.e.* by first synthesizing the hexagonal phase and then converting it to a perovskite structure through high-pressure treatment.

We here report the synthesis of a complete series of the hexagonal RMnO$_3$s (R = Sc, Y, Ho-Lu) and their high-pressure (HP) conversion to the metastable perovskite RMnO$_3$s, which offers an opportunity to observe the evolution of structural and magnetic properties within both the series as a function of the ionic radius $r(R^{III})$. Additionally, a hexagonal InMnO$_3$ sample was prepared and its conversion to a perovskite phase was attempted with the same HP method.

2. Experimental

High-quality samples of RMnO$_3$ (R = Sc, Y, Dy-Lu) were synthesized in air using an EDTA method [12] and the hexagonal RMnO$_3$ (except for R = Dy) phases were then converted to the corresponding orthorhombic perovskite phases through a HP treatment. Although the DyMnO$_3$ sample already had an orthorhombic structure as synthesized under normal condition, it was also treated under high pressure in order to see the effects of a HP treatment on the orthorhombic perovskite. Stoichiometric amounts of the starting materials, *i.e.* R_2O_3 (R = Sc, Y, Dy-Lu) and MnCO$_3$, were dissolved in diluted nitric acid. This solution was added slowly to an NH$_3$-EDTA solution and the pH of the solution was adjusted to ~9. The resultant solution was clear. The molar ratio of EDTA and metal ions was set at 1.5 in order to assure quantitative complex formation. The solution was heated at ~200 °C until a viscous gel was formed. Upon further heating the gel spontaneously ignited forming a low-density product or ash. The ash was then ground in an agate mortar for about 10 min and calcined in air at 800 °C for 8 h. The first step of sample sintering was carried out in air at 1000 °C for 24 h. Most of the samples contained starting materials after the first sintering and therefore the sintering was repeated at 1300 °C with intermediate grindings until the samples became phase-pure. Hexagonal InMnO$_3$ could not be prepared using the EDTA method and therefore an encapsulation technique was employed [25]. A stoichiometric mixture of the starting materials, In_2O_3 and Mn_2O_3, was ground in an agate mortar for an hour, and pressed into pellets which were then sealed in an evacuated quartz tube together with Mn_3O_4 as an oxygen getter. Such an oxygen getter is used to adjust the oxygen partial pressure inside the tube through reacting with the released oxygen, and Mn_3O_4 was chosen for the present case according to the Ellingham diagram [26]. The encapsulated samples were fired at 1000 °C for 48 h. In addition to the aimed h-InMnO$_3$ phase, In_2O_3 was found as an impurity in the resultant samples. A specimen was separated from all the hexagonal-phase samples and sealed in a gold capsule and treated in a cubic-anvil-type HP apparatus at 5 GPa and 800 °C for 30 min.

The samples were characterized by X-ray powder diffraction (XRD; Rigaku: RINT2550VK/U equipped with a rotating copper anode; Cu Kα radiation) at room temperature for phase purity and structural identification. For R = Er, Tm and Yb, minor amounts of unknown impurities, and for R = Lu, traces of Lu_2O_3 were detected in the XRD patterns. Magnetization was measured for the samples with a superconducting quantum interference device (SQUID) magnetometer (Quantum Design: MPMS-XL5) under a magnetic field of 1000 Oe in both field-cooled (FC) and zero-field-cooled (ZFC) modes. The measurement temperature was from 3 to 400 K for HoMnO$_3$ and from 5 to 400 K for the other RMnO$_3$ samples. In the case of HoMnO$_3$, the measurement was started from a lower temperature, because a magnetic transition of o-HoMnO$_3$ was anticipated at ~6 K.

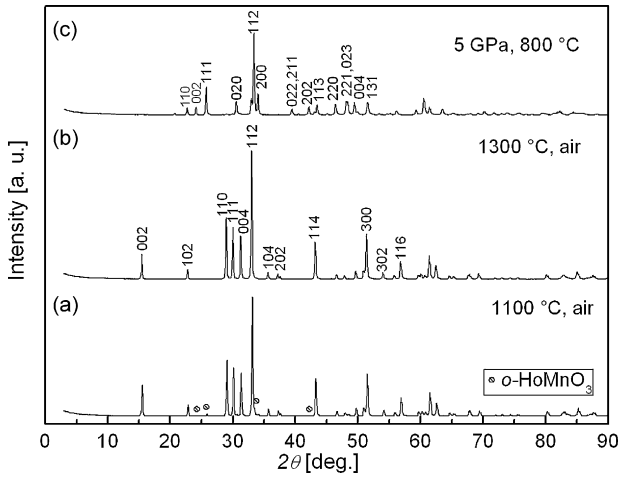

Fig. 1. XRD patterns of (a) the as-synthesized *h*-$HoMnO_3$ sample after sintering at 1100 °C, (b) the as-synthesized *h*-$HoMnO_3$ sample after sintering at 1300 °C and (c) the *o*-$HoMnO_3$ sample after HP treatment. The indices are for the hexagonal space group $P6_3cm$ (in (b)) and the orthorhombic space group *Pbnm* (in (c)).

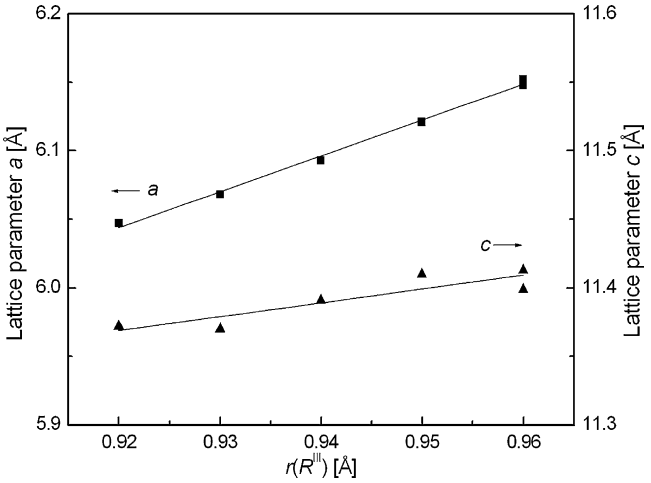

Fig. 2. Variation of the lattice parameters of *h*-$RMnO_3$ (*R* = Y, Ho-Lu) with the ionic radius, $r(R^{III})$. The ionic radii are for the 7-coordinated R^{III} ions [29,30].

The structure refinements based on the XRD data were performed with the FULLPROF software [27]. A Pseudo-Voigt function was chosen to generate the line shape of the diffraction peaks. The following parameters were refined: scale factor, background coefficients (6 terms), lattice parameters, zero-point error, positional coordinates, peak shape parameters, and asymmetry parameters. The occupancies and the atomic displacement parameters could not be refined. Although the *h*-$RMnO_3$ samples were of high quality, the refinement was done rather poorly. Similar problems have been encountered also in previous studies and it seems that neutron or synchrotron diffraction data are required to give an accurate profile for all the diffraction regions that are needed to refine a noncentrosymmetric structure, such as the hexagonal structure of *h*-$RMnO_3$ [19,28]. Table 1 shows the refinement results for the hexagonal and orthorhombic phases of the $RMnO_3$ series. (The reliability factors for refinements of *h*-$InMnO_3$ and *h*-$ScMnO_3$ were quite poor and therefore only the lattice parameters are listed for these two samples.)

3. Results and discussion

The air-synthesized $RMnO_3$ samples with *R* = Sc, Y, Ho-Lu presented the structure of space group $P6_3cm$ and the $DyMnO_3$ sample was found to be of space group *Pbnm*, as anticipated. Interestingly, after the first sintering at 1100 °C the *h*-$HoMnO_3$ sample already contained a small amount of orthorhombic *o*-$HoMnO_3$ as seen in Fig. 1. The result is however reasonable as orthorhombic *o*-$HoMnO_3$ can be prepared both under high pressure and through a soft-chemistry route at low temperatures [14,15]. Sintering at 1300 °C caused the perovskite phase to disappear. During the HP treatment the crystal structure of the *h*-$RMnO_3$ samples changed to orthorhombic (*Pbnm*) (Fig. 1). The HP annealing had little effect on the crystal structure of the $DyMnO_3$ sample which remained orthorhombic but got highly oriented along the [1 0 0] direction. Due to the strong orientation, the refinement of the structural details was difficult and therefore, in further comparisons of the structural details, only the data for the air-synthesized $DyMnO_3$ sample is considered. The conversion of hexagonal *h*-$InMnO_3$ and *h*-$ScMnO_3$ to the orthorhombic perovskite phases proved to be infeasible. Apparently the ionic radii of In^{III} and Sc^{III} are too small for the A site of the perovskite structure.

The lattice parameters of the hexagonal and orthorhombic samples are plotted in Figs. 2 and 3, respectively. The lattice parameters of both the polymorphs decrease monotonically as the size of the constituent rare earth decreases. In the hexagonal *h*-$RMnO_3$s, trimerization of the Mn^{III} ions leads to displacements of various atoms: the tilting of the MnO_5 polyhedra and the buckling of the *R* plane [18]. The buckling of the *R* plane is shown by the difference of the *z* position of two inequivalent *R* sites, $\Delta z \equiv z_{R1} - z_{R2}$ (Fig. 4). As can be seen, the buckling is enhanced with decreasing $r(R^{III})$. In the *o*-$RMnO_3$ series, on the other hand, orthorhombicity as defined by $(b-a)/b$ was found to increase with decreasing $r(R^{III})$ (Fig. 3). When the size of R^{III} decreases, the positions of oxygen atoms must be readjusted in order to maintain the connections with the *R* atoms. The distortion of the oxygen sublattice leads to increasing tilts of the MnO_6 octahedra, which, in turn, increases the orthorhombic splitting of the unit-cell dimension as compared to the ideal cubic perovskite structure. Furthermore, the progressive reduction in the R^{III} size in the orthorhombic *o*-$RMnO_3$ perovskite series also results in a decrease in the Mn—O—Mn angle. Fig. 5 shows the average Mn—O—Mn angle in *o*-$RMnO_3$ as a function of $r(R^{III})$. As seen in Fig. 5, the Mn—O—Mn angle does not change linearly. A considerable increase can be observed in the slope gradient for the three members with the largest rare earths (*i.e.* La, Pr and Nd). The $RMnO_3$ compounds with these rare earths are known to show oxidative nonstoichiometry [33,34]. However, this gives no explanation for our observation, as the data shown in Fig. 5 have been collected from stoichiometric samples [13,31]. To demonstrate the role of high pressure in the phase transformation, the densities of hexagonal and orthorhombic $RMnO_3$ phases were calculated. The unit-cell volumes used in the density calculations were obtained

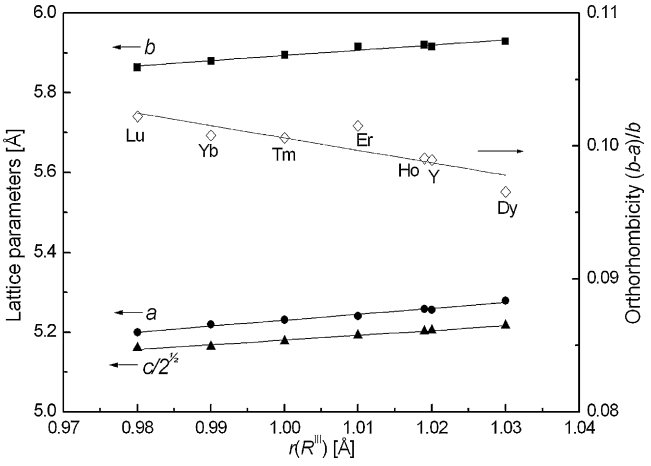

Fig. 3. Variation of the lattice parameters and degree of orthorhombicity of *o*-$RMnO_3$ (*R* = Y, Dy-Lu) with the ionic radius, $r(R^{III})$. The ionic radii are for the 8-coordinated R^{III} ions [29,30].

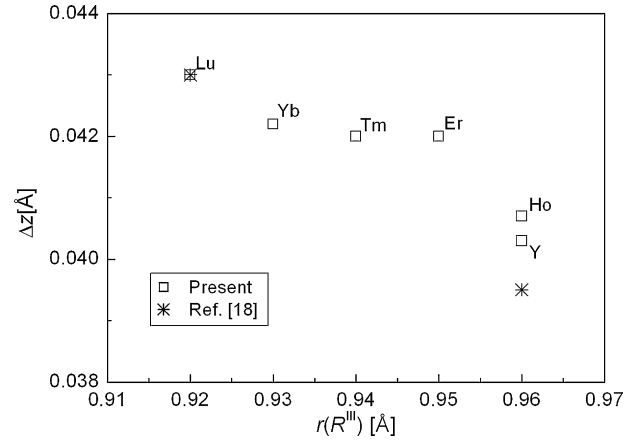

Fig. 4. Decrease in the magnitude of buckling of the R plane ($\Delta z = z_{R1} - z_{R2}$) in h-RMnO$_3$ (R = Y, Ho-Lu) with the ionic radius, $r(R^{III})$. The squares indicate the values observed in the present study and the stars show the results from an earlier report [18].

from the crystal structure refinements (Table 1). As seen in Fig. 6, the density increases considerably when the structure is converted from hexagonal to orthorhombic.

Fig. 7 presents the dependence of magnetic susceptibility (χ) on temperature (T) for hexagonal and orthorhombic RMnO$_3$s with R = Ho, Y, Tm and Lu. For both the polymorphs of TmMnO$_3$, there is

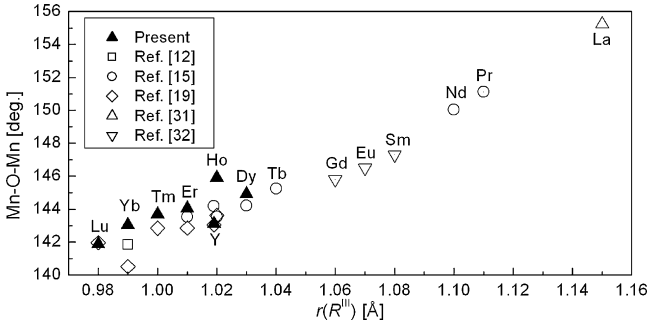

Fig. 5. Variation of the Mn—O—Mn bond angle of o-RMnO$_3$ with the ionic radius, $r(R^{III})$. The triangles indicate the values observed in the present study and the diamonds show the results from earlier reports [12,15,19,31,32].

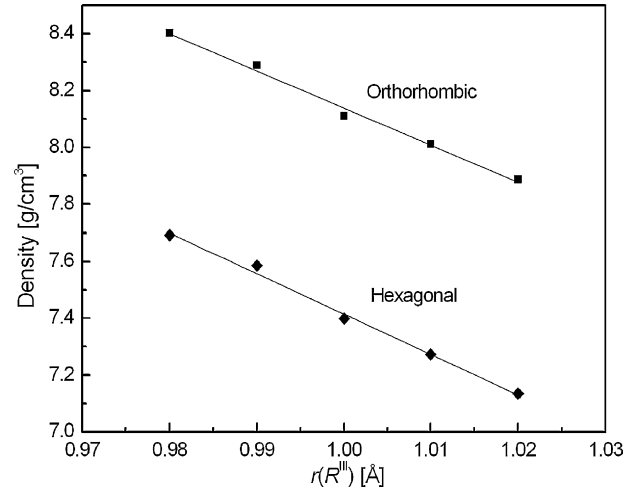

Fig. 6. The densities of hexagonal and orthorhombic RMnO$_3$ (R = Ho-Lu). The diamonds indicate the hexagonal and the squares indicate the orthorhombic phases. The ionic radii, $r(R^{III})$, are for the 8-coordinated R^{III} ions [29,30].

an anomaly in magnetic susceptibility at low temperatures. The thermal dependence of dχ/dT in the inset of Fig. 7 exhibits a magnetic transition of an antiferromagnetic type at 81 K for h-TmMnO$_3$, which is in good accordance with the reported Néel temperature for the AFM ordering of manganese moments in h-TmMnO$_3$ (T_N = 86 K) [35]. The magnetization curves for h-LuMnO$_3$ and h-YbMnO$_3$ show anomalies at 89 and 87 K, respectively. These values are consistent with previously reported Néel temperatures, *i.e.* 90 K for h-LuMnO$_3$ and 88 K for h-YbMnO$_3$ [35]. In the case of h-HoMnO$_3$, h-ErMnO$_3$ and h-YMnO$_3$, no apparent magnetic transitions were observed about T_N in the dχ/dT curves. Yoshii and Abe [35] have argued that the transitions in h-HoMnO$_3$ and h-ErMnO$_3$ are masked by the paramagnetism of Ho^{III} (effective paramagnetic moment μ_{eff} = 10.6 μ_B) and Er^{III} (μ_{eff} = 9.6 μ_B). However, this explanation cannot be valid for h-YMnO$_3$, because Y^{III} has zero magnetic moment. The magnetic transition temperatures for h-HoMnO$_3$, h-ErMnO$_3$ and h-YMnO$_3$ were estimated from the reciprocal magnetic susceptibility versus temperature curves, χ^{-1}/T. In all the cases, a linear relationship is observed above ~80 K. For o-YbMnO$_3$ and o-ErMnO$_3$ the dχ/dT vs. T curve exhibits an anomaly at 43 K. These observations are in accordance with previous results as the Néel temperature (T_N) has been reported to be 43 K for o-YbMnO$_3$ and 42 K for o-ErMnO$_3$ [12,36]. Magnetic transitions were observed at 43 K also for o-TmMnO$_3$ and o-YMnO$_3$. Orthorhombic o-LuMnO$_3$ undergoes a magnetic transition at 40 K. For o-HoMnO$_3$ and o-DyMnO$_3$, ordering of the manganese moments has been reported to occur at 38 and 39 K, respectively [37,38]. Nonetheless the dχ/dT vs. T curve for any of these phases does not exhibit an anomaly about this temperature; rather deviation from the Curie–Weiss behavior starts at ~40 K. Thus it can be concluded that T_N of the o-RMnO$_3$ perovskites with small Rs stays essentially constant as the ionic radius of R^{III} changes. The Néel temperatures for ordering of the manganese moments of both the polymorphs are summarized in Table 2. In the cases of o-HoMnO$_3$ and o-DyMnO$_3$, a maximum in magnetic susceptibility is observed at ~6 K and ~10 K, respectively. Such maxima are attributed to the antiferromagnetic interaction between the rare-earth ions [37,39].

The Curie–Weiss fitting for the temperature range between 150 and 400 K revealed a negative Weiss temperature (θ) for all the RMnO$_3$ samples (Table 2). The Weiss temperatures for hexagonal h-YbMnO$_3$ and h-LuMnO$_3$ are notably lower than those for other h-RMnO$_3$ compounds, but match reasonably well with the previously reported values, *i.e.* −200 K and −700 K, respectively [35]. The abso-

Table 2
Néel and Weiss temperatures together with the effective paramagnetic moments of hexagonal and orthorhombic RMnO$_3$

	Weiss temperature θ [K]	Néel temperature T_N [K]	Effective paramagnetic moment μ_{eff} [μ_B]	
Hexagonal ($P6_3cm$)			Observed	Theoretical
Ho	−20	~80	11.1	11.7
Y	−29	~80	8.9	4.9
Er	−29	~80	10.5	10.8
Tm	−61	81	8.6	9
Yb	−180	87	6.4	6.7
Lu	−602	89	5.2	4.9
Orthorhombic ($Pbnm$)				
Dy before HP	−20	~40	11.5	11.7
Dy after HP	−27	~40	11.6	11.7
Ho	−45	~40	12.4	11.7
Y	−118	43	5.7	4.9
Er	−20	43	10.7	10.8
Tm	−59	43	9.8	9.0
Yb	−72	43	6.9	6.7
Lu	−70	40	4.9	4.9

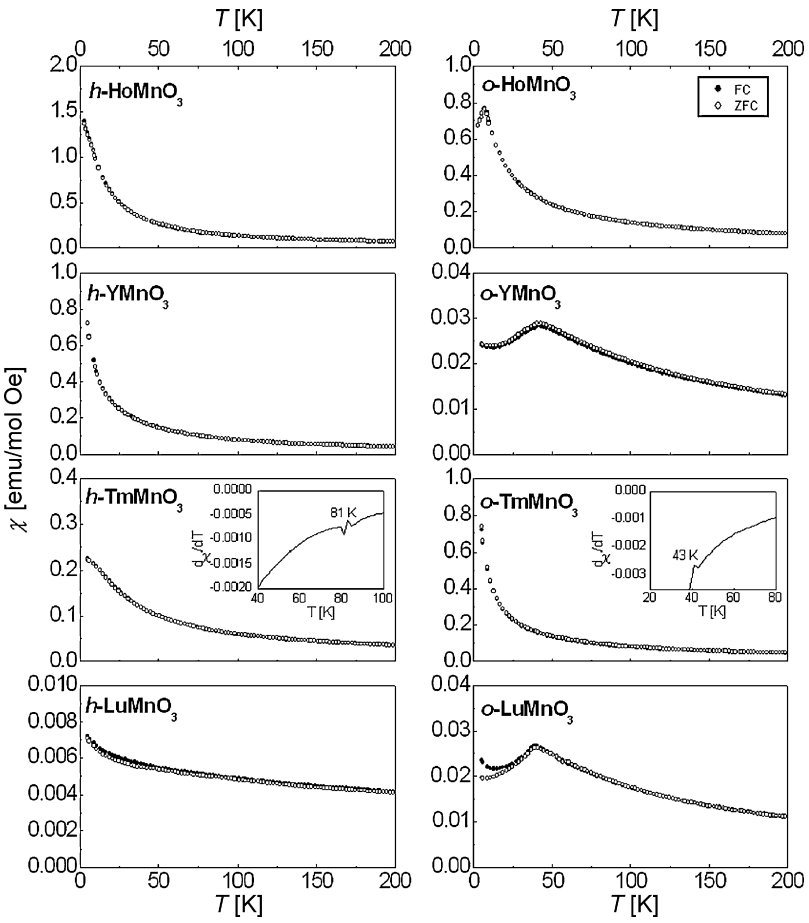

Fig. 7. Temperature dependence of magnetic susceptibility (χ) in ZFC and FC modes under an external field of 1000 Oe for hexagonal and orthorhombic RMnO$_3$ (R = Ho, Y, Tm and Lu).

lute value of θ for h-RMnO$_3$ seems to increase as $r(R^{III})$ decreases. This result may be explained by the strengthening of the magnetic interactions as the unit-cell volume decreases. For LuMnO$_3$ and YbMnO$_3$, the $|\theta|$ value was much higher compared to the corresponding Néel temperature. This phenomenon was attributed to the geometrical frustration in the two-dimensional triangular Mn–O lattice [35]. The Weiss temperatures of orthorhombic o-RMnO$_3$s are not likely to follow any specific trend and the values do not differ strongly from each other as in the case of h-RMnO$_3$s. However, as seen in Table 2, the effective paramagnetic moments of both the hexagonal and orthorhombic polymorphs investigated here increase with increasing $r(R^{III})$. In general, the values are also in excellent agreement with the theoretical values.

4. Conclusion

Firstly an entire sample series of the hexagonal RMnO$_3$ system was synthesized for R = Sc, Y, Ho-Lu, and then the samples were converted to orthorhombic o-RMnO$_3$ perovskites through a high-pressure (HP) treatment. The same HP treatment was found infeasible in conversing h-InMnO$_3$ and h-ScMnO$_3$ to perovskites. Thus, the stability limit with respect to the ionic radius, $r(R^{III}$ or $In^{III})$, of the orthorhombic perovskite structure under HP conditions was found between $r(In^{III})$ and $r(Lu^{III})$. A systematic study of the structural evolution showed that the lattice parameters of both polymorphs increase linearly as $r(R^{III})$ increases. The progressive reduction in the size of R^{III} increases the distortion of the o-RMnO$_3$ perovskites. The Mn—O—Mn bond angle was found to decrease from 144.3° for o-DyMnO$_3$ to 140.3° for o-LuMnO$_3$. The density of the RMnO$_3$ phase was found to increase considerably as the structure changes from hexagonal to orthorhombic, which makes it easy to understand why high pressure prefers the perovskite phase.

The hexagonal h-RMnO$_3$ phases showed an AFM ordering of the Mn moments at low temperatures. The Néel temperature was found to increase slightly from ~80 K (for h-HoMnO$_3$) to 89 K (for h-LuMnO$_3$) with decreasing $r(R^{III})$. All the orthorhombic o-RMnO$_3$ phases showed a magnetic transition of the AFM type around 40 K. Accordingly, the Weiss temperatures (θ) of h-RMnO$_3$ and o-RMnO$_3$ were negative. The absolute value of θ was found to increase as $r(R^{III})$ decreases and, for h-LuMnO$_3$ and h-YbMnO$_3$, the $|\theta|$ values are much higher than the Néel temperatures because of geometrical frustrations in the two-dimensional triangular Mn-O lattice. The θ values for orthorhombic o-RMnO$_3$s did not follow a specific trend, nor did they differ strongly from each other. However, the effective paramagnetic moments of both the hexagonal and orthorhombic polymorphs increase with increasing number of unpaired electrons. In general, the paramagnetic moments were in good agreement with the theoretically predicted values.

Acknowledgements

This work was supported by Academy of Finland (Decision Nos. 114517 and 116254), and also by MSL's International Collaborative Research Projects 2006 and 2007 (Tokyo Tech).

References

[1] H.Y. Hwang, S.-W. Cheong, P.G. Radaelli, M. Marezio, B. Batlogg, Phys. Rev. Lett. 75 (1995) 914.
[2] R. Von Helmolt, J. Wecker, B. Holzapfel, L. Schultz, K. Samwer, Phys. Rev. Lett. 71 (1993) 2331.
[3] Z.J. Huang, Y. Cao, Y.Y. Sun, Y.Y. Xue, C.W. Chu, Phys. Rev. B 56 (1997) 2623.
[4] M. Fiebig, Th. Lottermosser, D. Fröhlich, A.V. Goltsev, R.V. Pisarev, Nature 419 (2002) 818.
[5] T. Kimura, T. Goto, H. Shintani, K. Ishizaka, T. Arima, Y. Tokura, Nature 426 (2003) 55.
[6] F. Yen, C. dela Cruz, B. Lorenz, E. Galstyan, Y.Y. Sun, M. Gospodinov, C.W. Chu, J. Mater. Res. 22 (2007) 2163.
[7] L. Martín-Carrón, A. de Andrés, M.J. Martínez-Lope, M.T. Casais, J.A. Alonso, Phys. Rev. B 66 (2002) 174303.
[8] N.A. Spaldin, M. Fiebig, Science 309 (2005) 391.
[9] H.L. Yakel Jr., Acta Cryst. 8 (1955) 394.
[10] H.L. Yakel Jr., W.C. Koehler, E.F. Bertaut, F. Forrat, Acta Cryst. 16 (1963) 957.
[11] A. Waintal, J.J. Capponi, E.F. Bertraut, M. Contré, D. François, Solid State Commun. 4 (1966) 125;
A. Waintal, J. Chevanas Mater. Res. Bull. 2 (1967) 819.
[12] Y.H. Huang, H. Fjellvåg, M. Karppinen, B.C. Hauback, H. Yamauchi, J.B. Goodenough, Chem. Mater. 18 (2006) 2130.
[13] S. Quezel, J.R. Mignod, E.F. Bertaut, Solid State Commun. 14 (1974) 941.
[14] H.W. Brinks, H. Fjellvåg, A. Kjekshus, J. Solid State Chem. 129 (1997) 334.
[15] J.A. Alonso, M.J. Martínez-Lope, M.T. Casais, Inorg. Chem. 39 (2000) 917.
[16] P.A. Salvador, T.-D. Doan, B. Mercey, B. Raveau, Chem. Mater. 10 (1998) 2592.
[17] A.A. Bosak, A.A. Kamenev, I.E. Graboy, S.V. Antonov, O.Yu. Gorbenko, A.R. Kaul, C. Dubourdieu, J.P. Senateur, V.L. Svechnikov, H.W. Zandbergen, B. Holländer, Thin Solid Films 400 (2001) 149.
[18] T. Katsufuji, M. Masaki, A. Machida, M. Moritomo, K. Kato, E. Nishibori, M. Takata, M. Sakata, K. Ohoyama, K. Kitazawa, H. Takagi, Phys. Rev. B 66 (2002) 134434.
[19] J.-S. Zhou, J.B. Goodenough, J.M. Gallardo-Amores, E. Morán, M.A. Alario-Franco, R. Caudillo, Phys. Rev. B 74 (2006) 14422.
[20] M. Tachibana, T. Shimoyama, H. Kawaji, T. Atake, E. Takayama-Muromachi, Phys. Rev. B 75 (2007) 144425.
[21] T. Kimura, S. Ishihara, H. Shintani, T. Arima, K.T. Takahashi, K. Ishizaka, Y. Tokura, Phys. Rev. B 68 (2003) 60403.
[22] J.-W.G. Bos, B.B. van Aken, T.T.M. Palstra, Chem. Mater. 13 (2001) 4804.
[23] N. Imamura, M. Karppinen, H. Fjellvåg, H. Yamauchi, Solid State Commun. 140 (2006) 386.
[24] D.M. Giaquinta, H.-C. Zur-Loye, J. Am. Chem. Soc. 114 (1992) 10952.
[25] J.E. Greedan, M. Bieringer, J.F. Britten, J. Solid State Chem. 116 (1995) 118.
[26] F.D. Richardson, J.H.E. Jeffes, J. Iron Steel Inst. 160 (1948) 261.
[27] J. Rodríguez-Carvajal, Phys. B 192 (1993) 55.
[28] B.B. Van Aken, T.T.M. Palstra, Phys. Rev. B 69 (2004) 134113.
[29] R.D. Shannon, Acta Cryst. A 32 (1976) 751.
[30] Y.Q. Jia, J. Solid State Chem. 95 (1991) 184.
[31] J. Rodriguez-Carvajal, M. Hennion, F. Moussa, A.H. Moudden, L. Pinsard, A. Revcolevschi, Phys. Rev. B 57 (1998) R3189.
[32] T. Mori, N. Kamegashira, K. Aoki, T. Shishido, T. Fukuda, Mater. Lett. 54 (2002) 238.
[33] B.C. Tofield, W.R. Scott, J. Solid State Chem. 10 (1974) 183.
[34] H. Okamoto, H. Fjellvåg, H. Yamauchi, M. Karppinen, Solid State Commun. 137 (2006) 522.
[35] K. Yoshii, H. Abe, J. Solid State Chem. 165 (2002) 131.
[36] F. Ye, B. Lorenz, Q. Huang, Y.Q. Wang, Y.Y. Sun, C.W. Chu, J.A. Fernandez-Baca, P. Dai, H.A. Mook, Phys. Rev. B 76 (2007), 060402(R).
[37] H.W. Brinks, J. Rodríguez-Carvajal, H. Fjellvåg, A. Kjekshus, B.C. Hauback, Phys. Rev. B 63 (2001) 94411.
[38] R. Feyerherm, E. Dudzik, N. Aliouane, D.N. Argyriou, Phys. Rev. B 73 (2006) 180401.
[39] M. Mouallem-Bahout, O. Peña, D. Gutierrez, P. Duran, C. Moure, Solid State Commun. 122 (2002) 561.